Materials Letters 148 (2015) 71–75

Contents lists available at ScienceDirect

Materials Letters

journal homepage: www.elsevier.com/locate/matlet

Surface characterization, electrochemical behaviour and cytotoxicity of UNS S31254 stainless steel for orthopaedic applications

Mónica Luisa Chaves de Andrade Afonso [a], Ruth Flavia Vera Villamil Jaimes [b], Pedro A.P. Nascente [c], Sizue Ota Rogero [d], Silvia Maria Leite Agostinho [b,*]

[a] Instituto de Telecomunicações, Instituto Superior Técnico, Torre Norte-piso 10. Av. Rovisco Pais, 1, 1049-001 Lisboa, Portugal
[b] Instituto de Química, Universidade de São Paulo, Av. Prof. Lineu Prestes, 748, 05508-900 São Paulo, SP, Brazil
[c] Universidade Federal de São Carlos, Departamento de Engenharia de Materiais, via Washington Luis, Km 235, 13565-905 São Carlos, SP, Brazil
[d] Instituto de Pesquisas Energéticas e Nucleares, Av. Prof Lineu Prestes, 2242,05508-000 São Paulo, SP, Brazil

ARTICLE INFO

Article history:
Received 16 October 2014
Accepted 31 January 2015
Available online 11 February 2015

Keywords:
254 stainless steel
Sodium chloride
Orthopaedic implants

ABSTRACT

The surface characterization and electrochemical behaviour of UNS S31254 (254 SS) have been performed in 0.15 mol L^{-1} NaCl medium in order to evaluate its application as orthopaedic implants. Polarization curves, chronoamperometry, electrochemical impedance spectroscopy and X-ray photoelectron spectroscopy were used for characterizing the samples. A cytotoxicity test was also performed to study the biocompatibility of the proposed steel as biomaterial. The electrochemical behaviour of 254 SS was compared to that observed for ISO 5832-9 and ASTM F138 stainless steels, used in orthopaedic implants. 254 SS is similar to ISO 5832-9 SS: it is passivated on the potential range between the corrosion and the transpassivation potential. Mo (VI) forms an outer layer which blocks Cr (VI) dissolution. Cytotoxicity test showed no cytotoxic character of 254 SS.

1. Introduction

Austenitic stainless steels are used as internal fixation devices. Regardless of the lower corrosion resistance when compared to titanium, they exhibit excellent mechanical properties and low cost when compared to that material [1–2]. A new generation of steels with higher corrosion resistance and improved mechanical properties is being studied [3–7]. ISO 5832-9 SS is an example of steel used in orthopaedic implants. It does not suffer pitting corrosion contrarily to F 138-92 SS [8–9]. UNS S31254 SS (254SS) is highly resistant to corrosive media, such as hydrochloric acid [10], phosphoric acid [11] and does not present pitting potential in chloride media at room temperature [10]. The viability of the scientific investigation of 254SS for this purpose is also due to its high content of nitrogen [12].

This paper reports on the electrochemical characterization of 254SS in 0.15 mol L^{-1} NaCl at 37 °C from linear voltammetry, chronoamperometry, electrochemical impedance spectroscopy and X-ray photoelectron spectroscopy (XPS). Cytotoxicity test was also performed to evaluate its viability as orthopaedic implants. A comparative study between 254SS, ISO 5832-9 SS and ASTM F138 SS was also included.

2. Experimental

The chemical composition of the SS samples studied is given by: UNS S31254-19.40Cr, 17.70Ni, 6.26Mo, 0.52Si, 0.208N, 0.018P, 0.016C, 0.004S; ISO 5832-9- 20.70Cr, 9.94Ni, 2.50Mo, 0.33Si, 0.32N, 0.28Nb, 0.014P, 0.015C, 0.005S; ASTM F138-92-17.60Cr, 14.20Ni, 2.08Mo, 0.26Si, 0.023P, 0.021N, 0.012C, 0.002S.

The working electrodes (0.28 cm^2 area) were constructed according to previous descriptions [4]. The surface treatment of these electrodes was described elsewhere [4]. The auxiliary electrode consisted of a platinum foil and the reference electrode was the saturated calomel electrode (SCE). NaCl pa was used as electrolyte. All the experiments were conducted with naturally aerated solutions at (37.0 ± 0.5)°C. The electrochemical measurements were made using equipments described elsewhere [4]. Prior to each experiment the electrodes were immersed in the electrolyte until the attainment of the stationary open circuit potential (corrosion potential E_{corr}). The breakdown potential (E_B) was considered when the current density was equal to 10 μA cm^{-2} in the potentiostatic curves. The impedance measurements were performed from 100 kHz to 50 mHz, using 10 mV amplitude. The results were modelled using Boukamp's equivalent circuit.

The samples were analysed using a Kratos XSAM HS spectrometer from the same surface treatment used for the electrochemical measurements. The technique was performed for three conditions: 1st – after polishment (600 mesh), 2nd – after application of a potential in the passive region (E=300 mV/SCE) during 20 min

* Corresponding author.
E-mail address: smlagost@iq.usp.br (S.M.L. Agostinho).

http://dx.doi.org/10.1016/j.matlet.2015.01.157
0167-577X/

3rd – after application of $E=1400$ mV/SCE (transpassivation region) during 20 min. It was used ultrahigh vacuum (low 10^{-9} Torr range), a dual Mg/Al anode as X-ray source, emitting AlKα ($h\nu=1486.6$ eV) radiation with the application of 10 mA and 14 kV. High-resolution spectra were recorded at a normal emission angle using 20 eV analyser pass energy. The Shirley background, Gaussian (for 1s peaks) and mixed Gaussian/Lorentzian (for p and d peaks) functions, and a least-square routine were used for peak fitting. The binding energies were referenced to the adventitious hydrocarbon C 1s level set at 284.8 eV.

The cytotoxicity assay was carried out using the same procedure described elsewhere [4].

3. Results and discussion

The polarization curves are shown in Fig. 1.a. The electrochemical behaviour of 254 is similar to ISO 5832-9: both exhibit a wide potential range with passive film without evidence of pitting corrosion when compared to F 138SS. The passive region is characterized by current densities equal to $(1.50\pm0.01)\mu A\,cm^{-2}$; $(2.1\pm0.1)\mu A\,cm^{-2}$ and $(4.70\pm0.01)\mu A\,cm^{-2}$, at $E=0$ mV/SCE, 400 mV/SCE and 600 mV/SCE respectively. Its high resistance to pitting corrosion is attributed to the presence of Mo and N[13–14].

The voltammetric curve of 254SS is amplified in the passive region (Fig. 1.b). The anodic wave seen at about 750 mV can be attributed to oxidation of Cr(III) to Cr(VI) [15]:

$$Cr_2O_3+5H_2O\leftrightarrow 2CrO_4^{2-}+10H^++6e^-$$

However, the current density value corresponds to a passive film. At $E=1$ V a sharp increasing of the current can be seen due to the oxidation of Cr(III) and of the water without the presence of the passive film.

The results shown in Fig. 1.c corroborate the low currents suggested by polarization curve. Until $E=900$ mV/SCE current density values are lower than $10\,\mu A\,cm^{-2}$ and the transition between the passive to active behaviour takes place from $E=900$ mV/SCE ($j\approx10\,\mu A\,cm^{-2}$) to $E=950$ mV/SCE ($j\approx45\,\mu A\,cm^{-2}$).

The electrochemical impedance spectroscopy (EIS) was used to investigate the processes that occur on its surface at the corrosion potential and at more positive potentials (200, 400, 600, 800, 900, 950, 1000 and 1050)mV/SCE. The EIS measurements were performed after the electrode was held at open circuit potential for 15 min. The impedance spectra of 254 SS obtained are shown in Fig. 2.a and b. According to Nyquist plots at lower potentials, there is no significant change of the impedance diagrams, when the potential is increased from $E_{corr}=-20$ mV to $E=200$ mV. Bode plots at these potentials are similar: in the high frequency region the phase angle approaches 0, typical of a resistive behaviour. As the frequency diminishes a linear relationship can be observed between log (|Z|) and log (f) with a slope of -0.89 and approximately 80° phase angle, indicating a predominant capacitive behaviour typical of passive systems.

From $E=400$ mV/SCE to $E=900$ mV/SCE an arc is progressively formed and clearly seen at $E=900$ mV/SCE, the imaginary and real components of the impedance decrease with the increasing potential and the phase angle starts to diminish indicating that the film is loosening its protective behaviour. Impedance diagrams

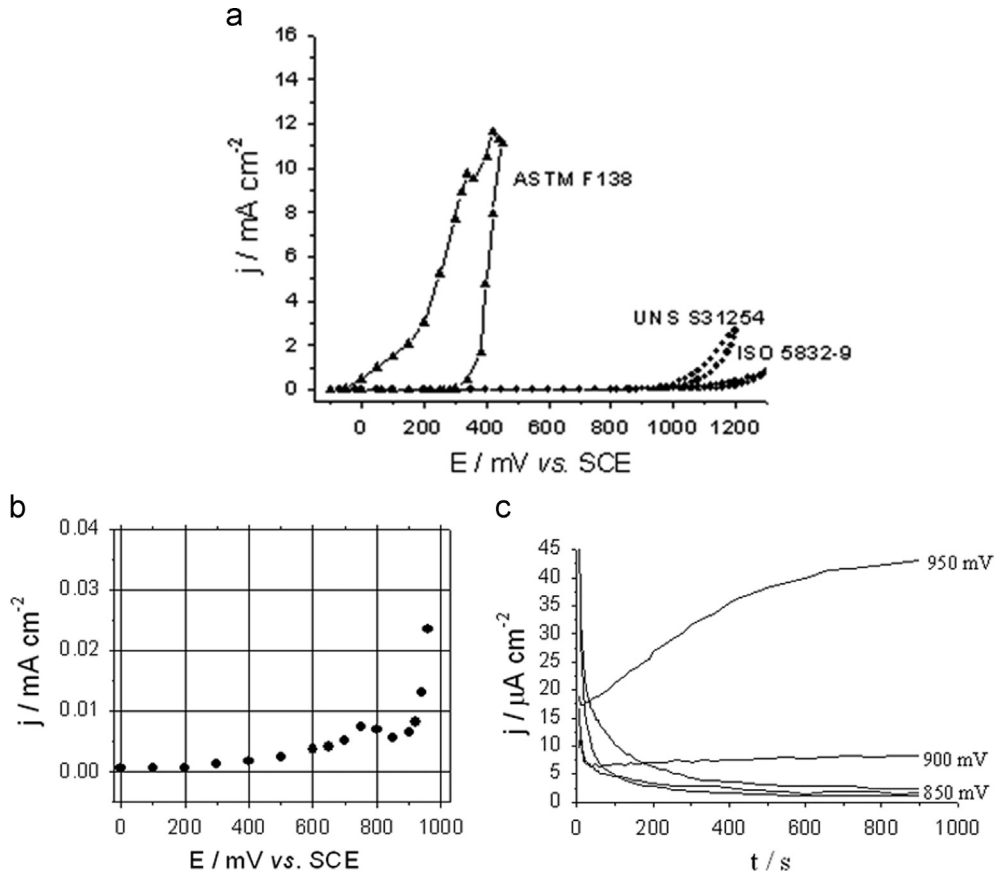

Fig. 1. (a) Polarisation curves of the stainless steels and (b) polarisation curve amplified in the passive region of 254 SS and (c) chronoamperograms of 254 SS in 0.15 mol L^{-1} NaCl medium at (37 ± 0.5) °C.

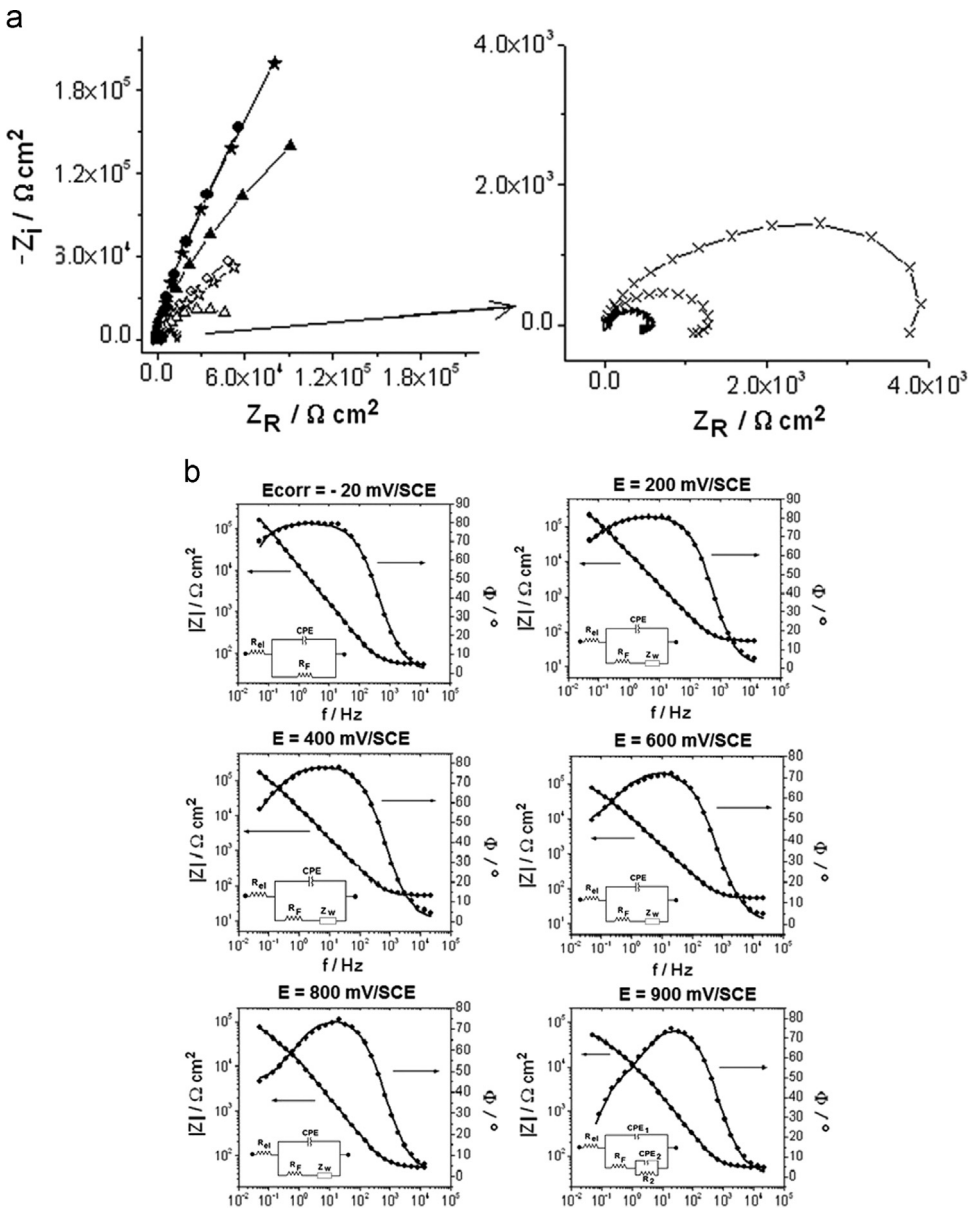

Fig. 2. Impedance diagrams for 254 SS in 0.15 mol L^{-1} NaCl medium at (37.0 ± 0.5) °C: (a) Nyquist plots at different potentials (•) E_{corr}, (★) 200 mV, (▲) 400 mV, (○) 600 mV, (◇) 800 mV, (△) 900 mV, (×) 950 mV, (*) 1000 mV and (▸) 1050 mV /SCE) at (37 ± 0.5)°C. (b) Bode plots registered at different potentials (E_{corr}, 200 mV, 400 mV, 600 mV, 800 mV, 900 mV. (•) experimental values, (—) simulation with electrical equivalent circuits used to fit the experimental data at different potentials.

of active systems with small values of Z_R and Z_i are observed at more positive potentials; the film is no longer protecting the surface.

The experimental results and simulation curves are shown in Fig. 2b. Fig. 2b presents the electrical circuits used to model the results. At E_{corr} the circuit is similar to that proposed by other authors for pure commercial titanium, titanium alloys and other stainless steels [4]. A frequency dependent constant phase element (CPE) was needed to reach a better agreement between experimental and simulated values [15,16–19]. The quality of fitting was judged by the chi-square value equal to 0.001. At $E_{corr} < E < 900$ mV/CSE a Warburg impedance models the experimental results pointing to diffusive processes. At $E = 900$ mV/SCE a cascade equivalent circuit with two time constants model the experimental data suggesting the existence of a bilayered film, an internal more compact layer and a less resistant outer layer or porous layer. In fact it was seen that at this potential the oxidation of Cr(III) to Cr(VI) has already begun (Fig. 1b). The two time constants can be attributed to different processes occurring simultaneously on the electrode surface. Current density values are still typical of passivated materials. At higher potentials it was not possible to find an acceptable fit due to oxygen evolution. At $E = 900$ mV/SCE the exponent of both the constant phase elements suggest absence of diffusive processes. The results obtained by EIS agree with those obtained by other techniques. EIS suggests the existence of diffusion processes through the passive film in the passive potential region. X-ray photoelectron spectroscopy (XPS) was performed to identify the species present in the passive film. XPS results are presented in Table 1. Both the grinded and the polarised ($E = 400$ mV/SCE) surfaces contain Fe, Cr, Ni and Mo as metal and as different oxides. In the polarized steel the content of Cr_2O_3 (576.3 eV binding energy) diminishes and the content of MoO_3 (232.9 eV binding energy) increases when compared to the grinded steel. This is in accordance with other authors [16–19], which have suggested the partial substitution of Cr by Mo in the passive film. Furthermore, this oxide suggests the existence of

Table 1
X-ray photoelectron spectroscopy (XPS) results for 254 SS.

(a) Binding energy / eV

	C 1s	O 1s	Fe 2p3/2	Cr 2p3/2	Ni 2p3/2	Mo 3d5/2
Grinded steel	284.8 (63%)	529.7 (45%)		573.6 (8%)		227.5 (32%)
			706.5 (12%)		852.3 (56%)	
	286.5 (17%)	531.3 (45%)		576.3 (92%)		229.2 (18%)
			708.3 (20%)		853.8 (15%)	
	288.4 (15%)	533.0 (10%)				232.9 (22%)
			710.6 (68%)		855.4 (29%)	
	289.9 (5%)					
Polarised steel (300 mV/SCE)	283.0 (3%)	529.8 (33%)		573.6 (11%)		227.4 (18%)
			706.5 (25%)		852.4 (63%)	
	284.8 (56%)	531.4 (51%)		576.3 (89%)	855.1 (37%)	229.0 (9%)
			708.8 (25%)			
	286.4 (22%)	533.0 (16%)				231.0 (8%)
			710.5 (50%)			
	288.4 (13%)					232.3 (65%)
Polarised steel (140 mV/SCE)	282.0 (9%)	528.3 (4%)	710.8	576.7		232.6
					852.7 (11%)	
	284.8 (56%)	530.0 (49%)				
					855.2 (89%)	
	287.0 (9%)	531.5 (40%)				
	289.1 (15%)	532.2 (6%)				
	290.0 (11%)					

(b) Attribution of binding energies to the different chemical substances.

Element	Binding energy / eV	Substance	Oxidation state
Fe	706.5	Fe	0
	708.3–708.8	Fe_2O_4	+2,+3
	710.5–710.8	Fe_2O_3	+3
Cr	573.6	Cr	0
	576.5–576.7	Cr_2O_3	+3
Ni	852.3–852.7	Ni	0
	853.8	NiO	+2
	855.1–855.4	Ni_2O_3	+3
Mo	227.4–227.5	Mo	0
	229.0–229.2	MoO_2	+1
	231.0	MoO_4^{-2}	+6
	232.3–232.9	MoO_3	+6

molybdate ion in the passive film when the surface is in contact with the solution, since XPS was performed ex-situ. After 1400 mV/SCE the chromium oxide is converted to Cr(VI). Different authors have also suggested the existence of molybdate ion in the passive film [18–19]. One can suggest that the passive mechanism is dynamic with the diffusion of molybdenium (VI) from the metal-oxide interphase to form an outer layer of adsorbed ions.

A cytotoxicity test was conducted to study the biocompatibility of 254SS as biomaterial. The positive and negative controls were used to confirm the adequate performance of the test and/or to evaluate the results from a new material, as well as to control the cell sensitivity, extraction efficiency, and other parameters. The cell viability percentage was calculated with the average of optical density triplicate of each extract dilution in relation to cell control considered 100%. In Fig. 3 $IC_{50(\%)}$, cytotoxicity index, means the concentration of the extract which kills 50% of cell population. The sample that presents cell viability curve above $IC_{50(\%)}$ is considered no toxic and under $IC_{50(\%)}$ is extremely toxic. The 254SS did not present toxic effects even at 100% extract concentration. It demonstrated similar behaviour to negative control, both presenting the viability curves above the cytotoxicity index which means that the sample showed no cytotoxicity [3,20–21]. Comparable results were previously reported for ISO 5832-9 SS and F138 SS [3] and they were included in the Fig. 3. Only the positive control viability curve crossed cytotoxicity line presenting toxic effect with $IC_{50(\%)}$ of about 38, which means that the phenol solution, in a dilution of 38%, killed 50% of cells.

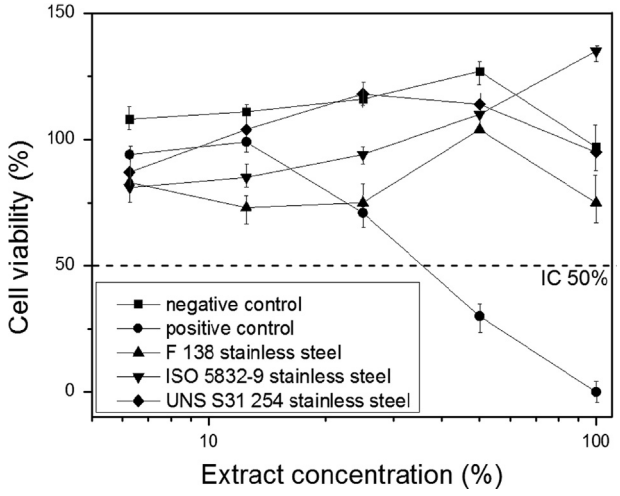

Fig. 3. F138 SS, ISO 5832-9 SS and 254 SS viability curves in the cytotoxicity assay by the neutral red uptake methodology.

It is important to note that in the previous work [3] the electrochemical behaviour of ISO 5832-9 SS and F138 SS was studied in MEM medium, and these materials presented the same behaviour observed in 0.15 mol L^{-1} NaCl, where these steels were compared to 254 SS.

4. Conclusions

The electrochemical behaviour of 254SS is similar to that observed for ISO 5832-9 SS and differently from F138 SS does not present localized corrosion: the passive region is characterized by low current density in a potential range of 1 V without pitting corrosion. Equivalent circuit model suggests that Mo(VI) forms an outer layer blocking the Cr(VI) dissolution. The 254SS cytotoxicity results pointed to the absence of toxic effect. The results permit to suggest the use of 254SS as biomaterial.

Acknowledgements

The authors thank FAPESP (Grant no. 01\10051-4), CNPq (Grant no. 200989\2011-1) and Adolfo Lutz Instiitute by cytotoxicity analysis, ASTM International, West Conshohocken, PA.

References

[1] Disegi JA, Eschbach L. Injury 2000;31:D2–6.
[2] Walczac J, Shahgaldi F, Heartley F. Biomaterials 1998;19:229–37.
[3] Jaimes RFVV Afonso MLCA, Rogero SO, Agostinho SML, Barbosa CA. Mater Lett 2010;64:1476–9.
[4] Salahinejad E, Hadianfard MJ, Macdonals DD, Sharifi-Asl S, Mosafari M, Walker KJ, et al. PLos One 2013;8(4):e61633.
[5] Rodrigues SF, Silva ES, Reis GS, Sousa RC, Balancin O. Mater Res 2014;17 (2):436–44.
[6] Giordani EJ, Guimarães VA, Pinto TB, Ferreira I. Int J Fatigue 2004;26:1129–36.
[7] Padilha AF, Machado IF, Plaut RL. Mater Process Technol 2005;170:89–96.
[8] Villamil RFV, Andrade AHP, Barbosa CA, Sokolowski A, Agostinho SML. In: Winters GL, Nutt MJ, editors. ASTM STP, 1438. West Conshohocken, PA: ASTM International; 2003. p. P168–75.
[9] Villamil RFV, Aranha H, Afonso ML, Mercadante MT, Agostinho SML. Rev Bras Ortop Traumatol 2002;37:471–9.
[10] Michelli L, Andrade AHP, Barbosa CA, Agostinho SML. Br Corros J 1999;34:67–70.
[11] Qvarfort R. Corros Sci 1989;29:987–93.
[12] Afonso MLCA Villamil Jaimes RFV, Arêas EPG, Capri MR, Oliveira E, Agostinho SML. Colloids Surf A: Physicochem Eng Asp 2008;317:760–3.
[13] Ilevbare GO, Burstein GT. Corros Sci 2003;45:1545–69.
[14] Doh SJ, Je JH, Kim JS, Kim KY, Kim HS, Lee YD, et al. Nucl Instrum Method B 2003;199:211–5.
[15] Li R, Ferreira MGS, Anjos MA, Vilar R. Surf Coat Tech 1997;88:90–5.
[16] Frateur I, Rojas L, Méthivier C, Galtayries A, Marcus P. Electrochim Acta 2006;51:1550–7.
[17] Boukamp B.. EQUIVCRT, Computer Software Analysis of Impedance Data, Technical version 4.51. 1998.
[18] Macdonald JR, editor. Impedance Spectroscopy. Ed Nova Iorque: Plenun; 1996.
[19] Bisquert J, Garcia-Belmonte G, Bueno P, Longo E, Bulhões LOS. J Electroanal Chem 1998;452:229–34.
[20] Rogero SO, Lugão AB, Ikeda TI, Cruz AS. Mat Res 2003;6:317–20.
[21] International Standard Organisation. ISO 10993- Biological evaluation of medical devices, part 5: Tests for *in vitro* cytotoxicity, 2009.